Infrared Radiative Transfer in Polluted Atmospheres[1]

THOMAS P. ACKERMAN

Department of Atmospheric Sciences, University of Washington, Seattle 98195

KUO-NAN LIOU

Department of Meteorology, University of Utah, Salt Lake City 84112

CONWAY B. LEOVY

Department of Atmospheric Sciences, University of Washington, Seattle 98195

(Manuscript received 17 March 1975, in revised form 8 September 1975)

ABSTRACT

A four-stream, multi-layered radiative transfer model has been developed to treat the problem of the transfer of infrared radiation in an atmosphere containing both scatterers and absorbers. Each atmospheric layer is isothermal and contains a uniform concentration of scatterers and absorbers. To facilitate the computations, the infrared spectrum was divided into four bands. In each band empirical transmission functions were fitted by a series of exponential functions. Test calculations of the infrared cooling rate were made using the empirical transmission functions and the fitted transmission functions. The resulting cooling rate profiles exhibit good agreement with each other. A model of a typical urban aerosol was developed using recent experimental results on the spectral dependence of the complex refractive index and the size distributions of aerosols. Atmospheric cooling rates as a function of height were computed on a band by band basis, with and without aerosols, in order to compare the effect of aerosols to the effect of H_2O and CO_2 in cooling the boundary layer. The presence of large, but realistic, concentrations of aerosol can substantially increase the infrared cooling of the aerosol-containing layer.

1. Introduction

In recent years, environmental concerns have prompted an interest in the effects of gaseous and particulate pollutants on the radiation budget of the earth-atmosphere system on both global and regional scales. The regional studies have generally been concerned with modeling polluted urban boundary layers, and considering the effect of increased aerosol loading on the net radiative flux in the boundary layer.

The scattering and absorption of visible radiation in homogeneous aerosol atmospheres has been treated quite accurately by previous investigators. In particular, Try (1972) used the Gauss-Seidel technique to solve the radiative transfer equation, and Bergstrom and Viskanta (1973a, b) used four-term polynomial expansions of both the phase function and the radiance to approximate the transfer solution. In both of these papers the authors include estimates of heating rates due to aerosol effects in the visible spectrum. The treatment of infrared radiation, however, has been considerably less comprehensive and complete. Atwater (1971a, b) and Bergstrom and Viskanta (1971a) employed broad-band flux emissivities for gases and single-scattering approximations for aerosols. Wang and Domoto (1974) extended the scattering calculations by means of a two-flux approximation.

The purpose of this paper is (i) to develop a reliable means of inserting gaseous absorption into the scattering computation and to verify such a technique based upon the calculation of atmospheric cooling-rates; (ii) to incorporate the non-isothermal structure of the atmospheric boundary layer into the radiative transfer program for aerosols and gases; and (iii) to investigate the relative significance of aerosol effects on various spectral regions in the infrared. In the present study the spectral dependence of the complex refractive index over the thermal infrared is incorporated into the radiation calculations using the recent measurements of Volz (1972a, b). Furthermore, realistic aerosol size distributions from recent intensive studies in Los Angeles (Hidy, 1972) and St. Louis (Dzubay and Stevens, 1975; Charlson *et al.*, 1974) are employed to evaluate the extinction properties of aerosols.

2. The radiative transfer model

The basic transfer equation for infrared radiation in an absorbing and scattering atmosphere may be written

[1] Contribution No. 342 from the Department of Atmospheric Sciences, University of Washington.

as

$$\mu\frac{dI_\nu(\tau,\mu)}{d\tau}=I(\tau,\mu)-\tfrac{1}{2}\tilde{\omega}_0\int_{-1}^{+1}d\mu' I_\nu(\tau,\mu')p_l(\mu,\mu')-(1-\tilde{\omega}_0)B_\nu(T), \quad (1)$$

where I_ν denotes the radiance (intensity), τ the optical depth, μ the cosine of the zenith angle, B_ν the Planck function, $p_l(\mu,\mu')$ the azimuthally averaged phase function, and $\tilde{\omega}_0$ is the single-scattering albedo which may be expressed as

$$\tilde{\omega}_0=\frac{b_s^a}{b_e^a+\kappa_\nu}. \quad (2)$$

In Eq. (2), b_s^a and b_e^a represent the scattering and extinction coefficients respectively due to aerosols, and κ_ν is the absorption coefficient due to gases. Molecular scattering is not included in this treatment because of its small contribution in the infrared spectrum.

Following the discrete-ordinate method of Chandrasekhar (1950) as developed by Liou (1973, 1974a, b), the phase function is expanded as a sum of Legendre polynomials, $P_l(\mu)P_l(\mu')$, and the integral in Eq. (1) is replaced by a sum using a Gauss-Legendre quadrature. The number of terms in the quadrature defines the number of discrete-ordinates or "streams," which will be used in calculating the radiative flux. In an earlier paper, Liou (1973) has illustrated that a four-stream method gives flux transmissivities and reflectivities correct in absolute differences to about 0.01 (or to 5% or less) when compared to more exact techniques. Since the four-stream method can be derived in an analytic form (Liou, 1974b), while higher order streams cannot, the use of four streams for computational purposes is advantageous in terms of both computer time and mathematical simplicity. This use of four streams also limits the number of terms in the polynomial expansion of the phase function to four in order to have a mathematically closed system. In terms of discrete-streams, Eq. (1) may be written as

$$\mu_i\frac{dI_\nu(\tau,\mu_i)}{d\tau}=I_\nu(\tau,\mu_i)-\tfrac{1}{2}\sum_{l=0}^{3}\tilde{\omega}_l P_l(\mu_i)\sum_j a_j I_\nu(\tau,\mu_j)P_l(\mu_j)-(1-\tilde{\omega}_0)B_\nu(T), \quad i,j=\pm1,\pm2, \quad (3)$$

where

$$\tilde{\omega}_l=\frac{(2l+1)}{2}\int_{-1}^{+1}P_l(\mu')p(\mu,\mu')d\mu', \quad (4)$$

and a_j and μ_j are the quadrature weights and roots, respectively. Note that Eq. (3) consists actually of four equations, because $i=\pm1, \pm2$. For an isothermal layer of temperature T, Eq. (3) admits a solution of the form

$$I_\nu(\tau,\mu_i)=\sum_j c_j\phi_j(\mu_i)\exp(-k_j\tau)+B_\nu(T). \quad (5)$$

The eigenvalues k_j and the eigenfunctions $\phi_j(\mu_i)$ are functions of the scattering parameters $\tilde{\omega}_l$, while the constants c_j are to be determined by boundary conditions at the top and bottom of the isothermal layer.

To treat a non-isothermal layer, the total layer is divided into m sublayers, each of which is approximately isothermal with a mean temperature T_m. The $\phi_j^m(\mu_i)$ and k_j^m can be calculated for each sublayer from the properties of that layer, while the c_j^m are to be determined by equating each of the four streams independently at the sublayer interfaces, and by the boundary values at the top and bottom of the total layer. For m sublayers this process results in a system of $4m$ coupled, linear equations in $4m$ unknowns. The system is then solved by a matrix inversion technique to yield the values of the c_j^m. Since Eq. (3) is solved independently in each of the sublayers, aerosol concentrations, relative humidity, and other radiation parameters can be varied from sublayer to sublayer.

Calculations of the radiative intensity or flux are further complicated by the fact that the extinction parameters are frequency-dependent. However, flux is additive so that the flux for any spectral band may in principle be computed by dividing it into intervals such that the extinction parameters are essentially constants over each interval. Thus, the flux for the qth interval is given by

$$F_q(\tau)=[-2\pi\sum_j \mu_j a_j I_q(\tau,\mu_j)]\Delta\nu_q, \quad (6)$$

where $\Delta\nu_q$ is the width of the frequency interval, and to total flux for the band is obtained by summing over all the intervals.

3. Gaseous absorption

The derivation outlined in the preceding section assumes that the interaction of gaseous absorbers with infrared radiation can be expressed by the use of a transmission function of the form $\exp(-\kappa_\nu u)$, where κ_ν is a constant with respect to changing path length u. Unfortunately, the primary gaseous absorbers in the infrared, CO_2 and H_2O, exhibit complicated line absorption structures, which usually cannot be expressed in the simple form indicated above. In the window region of the spectrum (1200 to 750 cm^{-1}), however, the absorption coefficient of the water vapor continuum (Bignell, 1970) is given by

$$\kappa_\nu=\kappa_\nu^{(1)}p+\kappa_\nu^{(2)}e, \quad (7)$$

where $\kappa_\nu^{(1)}$ and $\kappa_\nu^{(2)}$ represent the absorption coefficients due to the atmospheric pressure p and water vapor pressure e, respectively. It is clear that κ_ν varies with height. Because the selective absorption in the window region is much smaller than the continuous absorption, we may insert (7) into (2) to calculate the single-scattering albedo and carry out the transfer program.

To evaluate the transfer of radiation over a spectral region consisting of absorption lines in aerosol atmospheres, a general approach has been employed to fit the transmission function of a band (Yamamoto *et al.*, 1970; Houghton and Hunt, 1971; Liou, 1974a; Lacis and Hansen, 1974) as follows:

$$T_{\Delta\nu}(u)=\frac{1}{\Delta\nu}\int_{\Delta\nu}e^{-\kappa_\nu u}d\nu\approx\frac{1}{I}\sum_{i=1}^{I}e^{-\kappa_i u}. \tag{8}$$

The κ_i may be thought of as a set of equivalent absorption coefficients, which describe the absorption properties of sub-spectral regions. As a result of the exponential fitting of the transmission function, we may calculate the single-scattering albedo and the total optical depth for each sub-spectral interval in an atmosphere containing gases and particulates. Consequently, the radiative transfer program described in Section 2 may be carried out. The κ_i were evaluated by dividing the spectrum into three bands, the H_2O 6.3 μm vibrational band (2150 to 1200 cm^{-1}), the CO_2 15 μm band (750 to 580 cm^{-1}), and the H_2O rotation band (580 to 165 cm^{-1}), and then fitting a sum of exponentials to the empirical transmission functions of Rodgers and Walshaw (1966) in each of these bands. A comparison of the values of the fitted and empirical transmission functions for the two water vapor bands for various values of the optical depth is shown in Fig. 1.

The fitting procedure outlined above does not take into account the effect of pressure and temperature variations on the absorption coefficients. In empirical transmission functions these effects are usually treated by calculating an effective optical path length, which is a function of the pressure and temperature along the path as well as the total amount of absorbing material. In order to carry out the fitting procedure, we assume a constant multiplicative factor. Since the purpose of the model was to investigate the effects of boundary layer aerosols, a temperature of 290 K and a pressure equal to the surface pressure were used in the calculations of the empirical transmission functions.

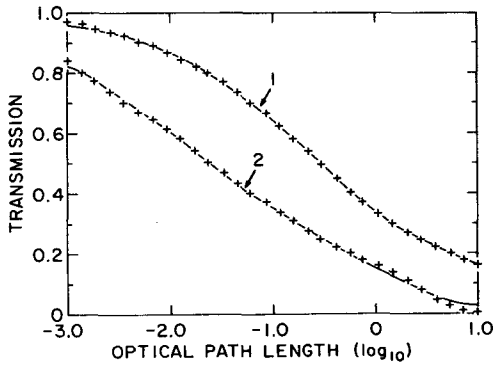

FIG. 1. Comparison of empirical transmission functions (solid curves) with fitted transmission functions (crosses) for two water vapor bands: 1, 6.3 μm band; 2, rotation band.

TABLE 1. Spectral intervals and equivalent absorption coefficients.

Spectral interval	Band	Interval midpoint (cm^{-1})	Width (cm^{-1})	κ_ν (g^{-1} cm^2)
1		2125.0	150	8.236×10^{-3}
2		2000.0	100	6.681×10^{-2}
3		1900.0	100	1.008
4	H_2O	1800.0	100	2.925
5	6.3 μm band	1700.0	100	1.522×10^{1}
6	(vibrational-	1600.0	100	1.522×10^{1}
7	rotational)	1500.0	100	2.488×10^{2}
8		1400.0	100	2.925
9		1275.0	150	3.823×10^{-1}
1	CO_2			2.347×10^{1}
2	15 μm band	667.0	170	2.428×10^{2}
3	(with H_2O overlap)			1.462×10^{3}
4				8.963×10^{1}
1		540.0	80	3.948×10^{-1}
2	H_2O	440.0	120	7.349
3	(rotation band)	330.0	100	6.716×10^{1}
4		220.0	120	8.098×10^{2}
				(1) κ_ν (2) κ_ν
1		1150.0	100	0.055 9.2
2	H_2O continuum	1050.0	100	0.07 9.0
3	(window)	950.0	100	0.10 12.0
4		825.0	150	0.16 22.0

The fitting process was simplified further by fitting each of the three bands with a sum of exponentials, rather than fitting each subinterval within the bands with a sum. The resulting κ_i were then arranged within the bands in such a way that the intervals with maximum absorption (empirically measured) have the largest κ_i values. The results of this process are shown in Table 1. While this procedure does not allow accurate calculations to be made on an interval by interval basis, the band totals from the exponential fitting accurately reflect the total absorption within the band.

In order to verify the results of the fitting procedure, cooling rate calculations were made using three different sets of transmission functions in the simple model of Rodgers and Walshaw (Fig. 2) for each of the three bands. The transmission functions used were (i) the empirical functions of Walshaw and Rodgers; (ii) these same functions but with a constant temperature of 290 K, and a constant pressure equal to the surface pressure used in the optical path calculations; and (iii) the fitted transmission functions. In all the cases the values of the atmospheric variables were taken from the T.1 sounding cited by Rodgers and Walshaw (1966). In both the 15 μm CO_2 band and the 6.3 μm H_2O band the cooling rate profiles are virtually identical below about 3 km. The agreement is not as good for the H_2O rotation band but is sufficient for the purpose of the model. The lack of agreement in the rotation band is due to the difficulty of modeling the complex line absorption and broad wings of this band with an expo-

nential fit. The use of smaller intervals and more terms in the exponential series would presumably increase the accuracy of the fit. The profiles of all three bands diverge somewhat in the region of 5 to 15 km due to the neglect of the pressure and temperature correction factors used by Rodgers and Walshaw. In fact, it is quite surprising that these corrections make so little difference on the cooling profiles shown in Fig. 2, and that the divergence of the profiles is so small. The divergence could be reduced by using a pressure scaling more applicable to this region or by using a matrix of κ_i values which would be functions of both frequency and pressure. The increased cooling evident about 20 km in the rotation band is a spurious result caused by truncation error in the computational scheme. For these calculations the top of the atmosphere was arbitrarily set at 30 km, and the downward radiation from the atmosphere above this level was neglected. The error caused by this effect below 20 km is negligible, and the error above 20 km can be reduced by moving the boundary higher in the atmosphere. This is a somewhat unsatisfactory solution because the method of Rodgers and Walshaw is not designed to be used at these high levels. Moreover, it is also difficult to calculate appropriate boundary conditions at these heights. Alternatively, the cooling-to-space approximation could be used to calculate upper level cooling rates. Similar comparisons were carried out for polar and equatorial soundings, as well as for a mid-latitude standard atmosphere, and gave equally good results.

4. Aerosol properties

To calculate the scattering parameters for the model it is necessary to compute the aerosol phase function.

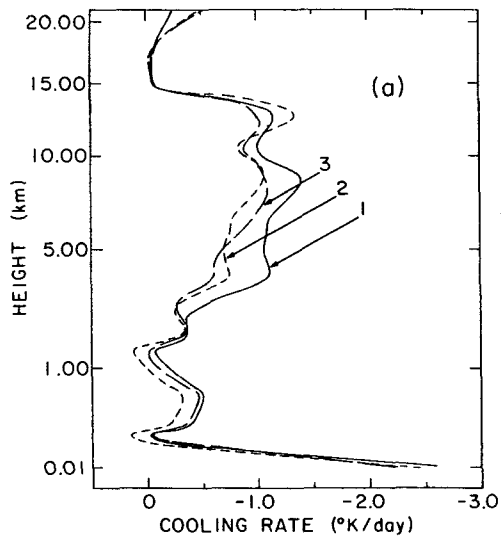

FIG. 2a. Comparison of cooling-rate profiles for the H_2O rotation band using Rodgers and Walshaw's method, 1, Rodgers and Walshaw's method with a fixed temperature of 290°K and a fixed pressure correction, 2, and Rodgers and Walshaw's method with fitted transmission functions, 3.

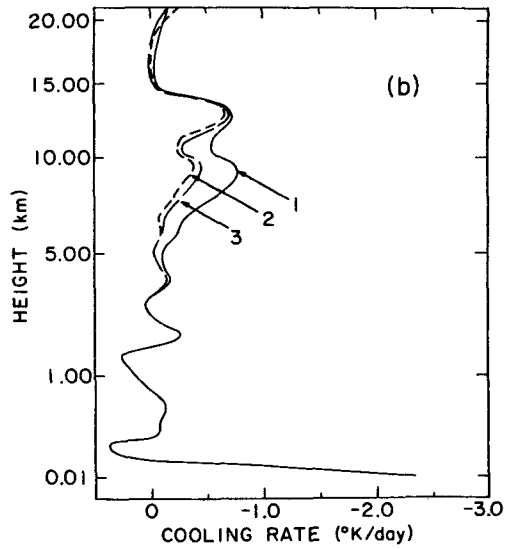

FIG. 2b. As in Fig. 2a except for the CO_2 15 μm band.

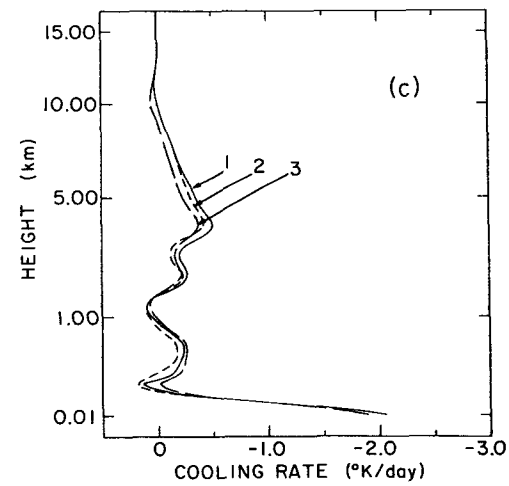

FIG. 2c. As in Fig. 2a except for the H_2O 6.3 μm vibration-rotation band.

This computation, based on Mie scattering theory, requires the knowledge of the aerosol size distribution and the frequency-dependent complex index of refraction. Although neither of these quantities is sufficiently well known so as to remove questions about their values, some recent intensive studies in Los Angeles (Hidy, 1972) and St. Louis (Dzubay and Stevens, 1973; Charlson *et al.*, 1974; Bhardwaja *et al.*, 1974) have provided enough information to draw a reasonably coherent picture of the composition and sizes of urban aerosols.

The aerosol model suggested by these data is that of a bi-modal size distribution (Whitby *et al.*, 1972) where the total mass of aerosol is roughly equally divided between the two modes, and where each of the modes can be fitted accurately by a log-normal distribution function. The larger mode has a modal radius

TABLE 2. Index of refraction for Sahara dust (large particles) and water-soluble aerosol (small particles) (after Volz, 1973).

λ (μm)	Large particles n_r	Large particles n_i	Small particles n_r	Small particles n_i
45.45	2.41	0.72	1.80	0.40
30.30	2.45	0.59	1.82	0.28
22.73	2.64	1.10	1.96	0.22
18.52	2.36	0.77	2.00	0.15
15.0	1.50	0.26	1.50	0.11
11.76	1.79	0.24	1.67	0.06
10.53	1.74	0.76	1.71	0.07
9.52	2.63	0.80	1.98	0.11
8.70	1.06	0.38	1.61	0.10
7.14	1.40	0.10	1.41	0.063
5.88	1.40	0.05	1.41	0.047
5.00	1.50	0.013	1.41	0.011

of the mass distribution in the range of 6–8 μm and has a fairly narrow standard deviation due to the large settling velocity of particles greater than 10–15 μm in radius. The particles in the large mode are predominantly of natural origin, and are composed primarily of silicon compounds from windblown dust. In coastal areas a sizable fraction of these particles may be composed of various sea salts. Studies of rock slices (Pollack *et al.*, 1973) and Sahara dust (Volz, 1973) provide good detailed values of the real and imaginary parts of the index of refraction of these larger particles (Table 2).

The smaller of the two modes has a modal radius of the mass distribution of about 0.2 μm, and is composed of particles which are predominantly of anthropogenic origin [e.g., sulfur and carbon compounds (Mueller, *et al.*, 1972; Novakov *et al.*, 1972); lead, zinc and arsenic salts; organic compounds of many varieties; and some inorganic acids (Schuetzle, 1972)]. Because many of the salts and acids are hygroscopic in nature, these particles also contain substantial amounts of water. This leads to the formation of other compounds, e.g. bisulfates and ammonium sulfate, in solution. Since the composition of these particles is so complex, the index of refraction of actual aerosol samples must be measured in order to get reasonable values for use in numerical models. Unfortunately, such measurements are rarely made at wavelengths in the infrared spectrum. The work of Volz (1972a, b) provides values for the water-soluble fraction of an urban aerosol, and these values are presently adopted in this paper to represent the anthropogenic aerosol fraction (Table 2). As mentioned previously, these particles are hygroscopic and consequently their properties are dependent on the relative humidity of the surrounding air (Covert *et al.*, 1972; Covert, 1974). Although the qualitative effect of changing relative humidity on aerosols has been documented, quantitative relationships have not been deduced, particularly for complex urban aerosols. Therefore we shall neglect the dependence of aerosol properties on relative humidity in this study.

The work of Dzubay and Stevens (1975) suggests that particles in different modes are essentially noninteracting. In this case, then, the total volume phase function can be written as a weighted sum:

$$p(\mu,\mu')=f_1p_1(\mu,\mu')+f_2p_2(\mu,\mu'), \tag{9}$$

where p_1 and p_2 are phase functions of the two types of scatterers, and f_1 and f_2 denote the ratios of the contribution of each type of scatterer to the total scattering cross section. Note that f_i is a function of the number density of the ith type of scatterer.

5. Some model calculations

The first calculation made with the four-stream model was for the purpose of determining the reliability of the model formulation. The model was run for ten layers ranging from the ground to 25 km and for the entire infrared spectrum. The calculated cooling rates were then compared with cooling rates calculated using both the fitted and the empirical transmission functions in the model of Rodgers and Walshaw. A comparison of these three calculations is shown in Fig. 3. All three methods give similar results in the lower 2 km. The four-stream model shows good agreement with the values computed using the fitted transmission function up to about 7 km. Above this level the two curves become increasingly divergent. This divergence is due

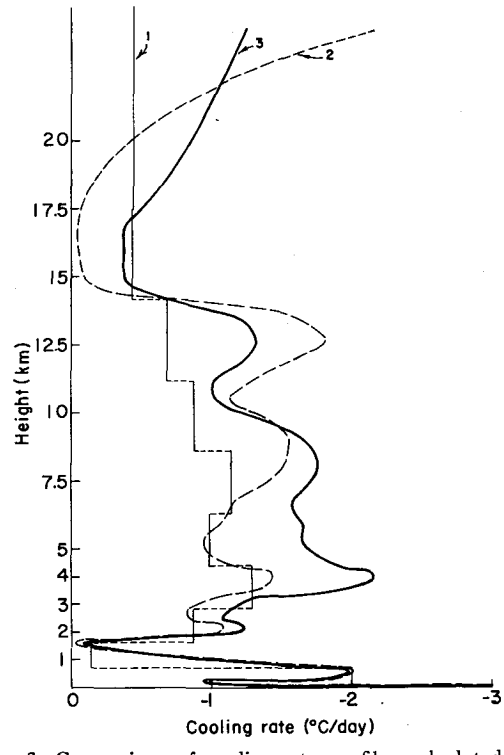

FIG. 3. Comparison of cooling-rate profiles calculated using the four-stream model, 1, Rodgers and Walshaw's method with fitted transmission functions, 2, and Rodgers and Walshaw's method with empirical transmission functions, 3.

to several causes. First of all, the four-stream method assumes that each sublayer can be described by a single temperature. Because fairly thick layers (2.5–4 km) were used in the region above 7 km and because there is a rather strong lapse rate in this region, it seems likely that a significant error in the flux calculation is introduced by assuming isothermal sublayers. Second, the four-stream values are strongly influenced in the upper levels by the boundary conditions chosen at the layer top because of the small amount of absorber in these upper levels. The boundary conditions were calculated using the method of Rodgers and Walshaw which is not particularly accurate at these high levels. And finally, the increase in cooling occurring above 20 km in curves 2 and 3 is due to truncation error and does not represent a real cooling. Subsequent calculations showed that this problem does not occur when the layer top for the four-stream model is placed below about 5 km. In this case, the sublayers are much thinner and consequently do a better job of representing the real atmosphere, and it is also easier to compute appropriate boundary conditions. As a result of these tests, we decided to place the model top at about 2 km and divide the region below this level into six layers to represent the actual atmosphere.

Following this initial model check, calculations were made to determine aerosol effects on the cooling rates. For these calculations an atmospheric sounding from San Diego and aerosol concentrations and size distributions from Los Angeles (Whitby *et al.*, 1972) were used. The sounding is fairly typical for late afternoon in southern California and exhibits a weak inversion occurring at about 960 mb. Three aerosol concentrations were used. The first, labelled light, is essentially a no-aerosol case with a concentration of 10^{-1} particles cm^{-3}. The second case is based on 342 size distributions measured in Los Angeles (Whitby *et al.*, 1972), and has an averaged number concentration of 10^5 cm^{-3}, while the third case is for heavy particulate loading and uses a concentration of 10^6 cm^{-3}. This latter case represents an occasional large number of small particles caused by combustion processes (Whitby *et al.*, 1972). Table 3 shows the values of some of the aerosol parameters based on these concentrations at a wavenumber of 1050 cm^{-1} (in the window region at 9.5 μm). Values of the complex index of refraction are given for both the large and small particles. $\tilde{\omega}_0(a)$ and $\tilde{\omega}_0(t)$ are the single-scattering albedos for the aerosol and for the aerosol plus gas system respectively. $\tilde{\omega}_1$ is the asymmetry factor and $\tilde{\omega}_2$ and $\tilde{\omega}_3$ are higher order moments of the phase function expansion. The numbers indicate that increasing aerosol concentration tends to increase the absorption fraction of the aerosol because $\tilde{\omega}_0(a)$ decreases. Increasing concentration also tends to produce isotropic scattering as shown by decreasing values of $\tilde{\omega}_1$. The continuum absorption coefficient κ_ν dominates $\tilde{\omega}_0(t)$ for low concentrations but it is only a few percent of the total extinction for the heaviest concentration.

TABLE 3. Aerosol extinction parameters for a wavenumber of 1050 cm^{-1} (9.5 μm) for various aerosol concentrations. (All the symbols are explained in the text.)

	Aerosol concentration		
	Light	Average	Heavy
n_r (large)	2.63	2.63	2.63
n_i (large)	0.80	0.80	0.80
n_r (small)	1.98	1.98	1.98
n_i (small)	0.11	0.11	0.11
$\tilde{\omega}_0$ (a)	0.4452	0.3827	0.3713
$\tilde{\omega}_1$	0.5360	0.3583	0.3192
$\tilde{\omega}_2$	0.3844	0.1946	0.1529
$\tilde{\omega}_3$	0.2639	0.0795	0.0389
κ_ν	1.89×10^{-6}	1.89×10^{-6}	1.89×10^{-6}
$\tilde{\omega}_0$ (t)	$<10^{-5}$	0.1977	0.3371
τ (1 km)	0.0788	0.227	1.395

The effect of increasing concentration is very noticeable in the value of the optical path length at 1 km, τ(1 km), which changes from optically thin ($\tau=0.079$) to optically thick ($\tau=1.4$) as the concentration increases.

Since the magnitude of the gaseous absorption varies so strongly over the infrared spectrum, the effect of aerosol extinction was investigated on a band by band basis in order to identify those bands where it might be significant. Not surprisingly, the effect of aerosol extinction is not observable in the 15 μm CO_2 band and is of negligible importance in the H_2O vibrational and rotational bands. The effect in the window region, however, is of considerable importance. The resulting calculations are shown in Table 4. In all cases but the last the excess cooling was calculated by comparing the light and the average concentration cases. Note that the last case uses the heavy aerosol concentration in place of the light. The vertical distribution of temperature, mixing ratio and aerosol concentrations employed in these calculations are shown in Table 5. The aerosol was confined to a layer below 1 km because of the inversion in the sounding. Consequently, the excess cooling averaged over the bottom kilometer is larger than the excess cooling averaged over the bottom 1.75 km.

A more detailed look at the effect of aerosols in the window region (Fig. 4) shows some interesting changes

TABLE 4. Cooling rates (K day^{-1}) for light and average aerosol concentrations for four infrared bands. Excess cooling denotes the increase in amount of cooling due to aerosol. $\overline{\Delta z}$ is the thickness of the layer over which the cooling is averaged.

Band	$\overline{\Delta z}$	Light	Average	Excess cooling
15 μm	1.75	−0.103	−0.103	0.0
6.3 μm	1.75	−0.550	−0.625	−0.075
Rotation	1.75	−0.479	−0.526	−0.047
Window	1.75	−1.008	−1.328	−0.320
Window	1.00	−1.667	−2.494	−0.827
Window	1.00	−1.667	−5.922 (heavy)	−4.255

TABLE 5. Parameter values for the six layers used in the cooling rate calculations. A surface temperature of 297.2 K is employed.

Layer	Δz (km)	$\bar{T}$ (°K)	$\bar{M}$ (g kg^{-1})	Average aerosol concentration (cm^{-3}) Large part	Small part	Heavy aerosol concentration (cm^{-3}) Large part	Small part
1	0.0–0.1	296.5	8.33	10^{-1}	10^{5}	1.5×10^{-1}	10^{6}
2	0.1–0.2	295.8	6.18	10^{-1}	10^{5}	1.5×10^{-1}	10^{6}
3	0.2–0.4	297.3	4.78	10^{-1}	15^{5}	1.5×10^{-1}	10^{6}
4	0.4–0.7	298.7	4.24	10^{-1}	10^{5}	1.5×10^{-1}	10^{6}
5	0.7–1.0	297.8	4.10	10^{-2}	10^{4}	10^{-2}	10^{4}
6	1.0–1.75	294.0	3.69	10^{-4}	10^{2}	10^{-4}	10^{2}

in the vertical profiles. For the light-aerosol concentration, cooling from the surface dominates the radiation process. For the average case, the cooling is spread more uniformly over the aerosol layer with a maximum at the surface. Because of the large optical depth, the heavy-aerosol concentration case shows a pronounced maximum in the model sublayer, which represents the top of the uniformly mixed boundary layer. On the basis of these latter calculations, it appears likely that an aerosol layer trapped below an inversion may act to strengthen the inversion by cooling from the top of the aerosol layer. This in turn would increase the aerosol concentration below the inversion by preventing the lifting or destruction of the inversion. We note that further modeling including solar radiation and convective heat transfer is needed to determine more completely the question as to whether the inversion is enhanced by an aerosol layer.

Finally, we investigate the net infrared flux at the ground. This quantity is of importance in both global climate modeling and regional heat-budget studies. Table 6 shows the change in the net upward flux at the ground for the various bands and aerosol concentrations. In this model the upward flux at the ground is simple σT_g^4. Consequently, any changes in the net flux are caused by changes in the downward flux. It is clear that the most substantial change occurs in the window region although there are some relatively minor variations occurring in the H_2O bands. Of course this decrease of net upward flux due to infrared blanketing is only one of the aerosol effects on the surface heat balance. The ground temperature and consequent upward flux at the ground would be expected to rise somewhat because of this blanketing alone. On the other hand, aerosols would reduce the solar radiation reaching the surface. The net effect of aerosols on the surface heat balance will depend on the aerosol modification of the convective heat flux as well as on the changes in net infrared and solar fluxes at the ground.

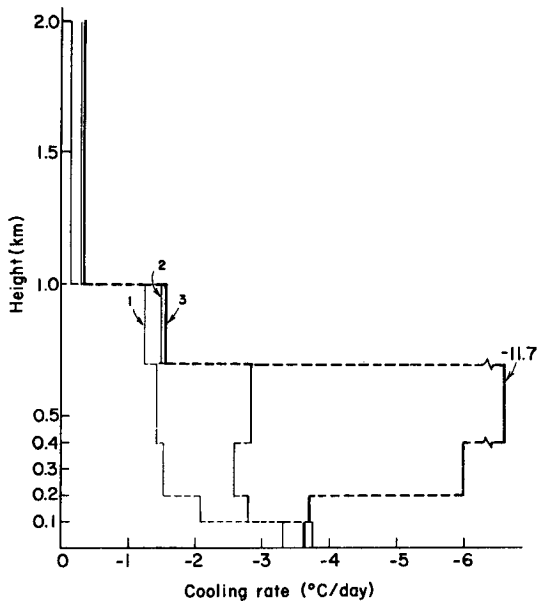

FIG. 4. Comparison of boundary-layer cooling-rate profiles for the light aerosol, 1, the average aerosol, 2, and the heavy aerosol, 3, in the lowest kilometer.

6. Conclusions

Comparison tests of both the fitted gas transmission functions and the transfer program indicate that the present model represents closely the infrared radiation in a scattering and absorbing atmosphere to a degree of accuracy commensurate with other uncertainties in the problem. Furthermore, we show that although aerosols produce insignificant influences in the bands which exhibit strong gaseous absorption, their effects are of considerable importance in the window region. Our results indicate that the presence of particulate matter in large quantities causes a substantial increase in atmospheric cooling. The amount of cooling is related to the amount of aerosol, the thickness of the

TABLE 6. Net flux (positive upward) at the ground for the different bands and aerosol concentrations (units, ergs cm^{-2} s^{-1}).

	Window region	6.3 μm band	15 μm band	Rotation band
Light aerosol	9.722×10^{4}	1.564×10^{4}	6.337×10^{2}	1.410×10^{4}
Average aerosol	8.334×10^{4}	1.359×10^{4}	6.337×10^{2}	1.290×10^{4}
Heavy aerosol	3.319×10^{4}	—	—	—

layer in which this material is contained, and the single-scattering albedo. For the typical case of a low-lying inversion at about 1 km and uniform aerosol concentration below that inversion, we find that the cooling in this layer can be on the order of 5 or 10 K per day. This is comparable with, but opposite in sign, to the heating of aerosol layers by absorption of solar radiation (Try, 1972), and is the same order of magnitude as the diurnal convective heating of the boundary layer. Thus we may expect considerable cancellation between the solar and infrared effects on the mean temperature of aerosol-containing layers. On the other hand, there may be a pronounced effect of aerosols on the diurnal temperature variation. One of us (TPA) is incorporating the technique employed here into a boundary layer model with both solar and infrared radiative effects in order to develop a more complete picture of the influence of urban aerosols and gases on changes in mean temperature, diurnal temperature variation, and the stability of low-level inversions. We also find that this type of aerosol layer tends to heat the ground surface by increasing the amount of downward infrared radiation reaching the ground. This of course is the opposite of the effect of aerosols on solar radiation. In view of the results cited above we suggest that aerosol effects on infrared radiation may play an important role in determining the total heat budget of the urban boundary layer and ought not to be neglected when solar effects are being considered. In addition, aerosol effects may influence the strength and position of inversions.

Acknowledgments. The authors are indebted to Dr. T. Sasamori for a number of useful discussions, and to Prof. H. Harrison for providing assistance on the computations of the fitting routine. This research was supported by the Atmospheric Sciences Section of the National Science Foundation under Grant DES75-05216 to the University of Utah and under Grant DES74-20207 to the University of Washington.

REFERENCES

Atwater, M. A., 1971a: The radiation budget for polluted layers of the urban environment. *J. Appl. Meteor.*, **10**, 205–214.

——, 1917b: Radiative effects of pollutants in the atmospheric boundary layer. *J. Atmos. Sci.*, **28**, 1367–1373.

Bergstrom, R. W., Jr., and R. Viskanta, 1973a: Modeling of the effects of gaseous and particulate pollutants in the urban atmosphere. Part I: Thermal structure. *J. Appl. Meteor.*, **12**, 901–912.

——, 1973b: Modeling of the effects of gaseous and particulate pollutants in the urban atmosphere. Part II: Pollutant dispersion. *J. Appl. Meteor.*, **12**, 913–918.

Bhardwaja, P. S., J. Herbert and R. J. Charlson, 1974: Refractive index of atmospheric particulate matter: An *in situ* method for determination. *Appl. Opt.*, **13**, 731–734.

Bignell, K. J., 1970: The water-vapor infra-red continuum. *Quart. J. Roy. Meteor. Soc.*, **96**, 390–403.

Chandrasekhar, S., 1950: *Radiative Transfer*. Dover, 393 pp.

Charlson, R. J., A. H. Vanderpol, D. S. Covert, A. P. Waggoner and N. C. Ahlquist, 1974: $H_2SO_4/(NH_4)_2SO_4$ background aerosol: Optical detection in St. Louis region. *Science*, **184**, 156.

Covert, D. S., 1974: A study of the relationship of chemical composition and humidity to light scattering by aerosols. Ph.D. thesis, University of Washington, 167 pp.

——, R. J. Charlson and N. C. Ahlquist, 1972: A study of the relationship of chemical composition and humidity to light scattering by aerosols. *J. Appl. Meteor.*, **11**, 968–976.

Dzubay, T. G., and R. K. Stevens, 1975: Ambient air analyses with dichotomous sampler and x-ray fluorescence spectrometer. *Environ. Sci. Tech.*, **9**, 663–668.

Hidy, G. M. Ed., 1972: *Aerosols and Atmospheric Chemistry*. Academic Press, 248 pp.

Houghton, J. T., and G. E. Hunt, 1971: The detection of ice clouds from remote measurements of their emission in the far infrared. *Quart. J. Roy. Meteor. Soc.*, **96**, 1–17.

Lacis, A. A., and J. E. Hansen, 1974: A parameterization for the absorption of solar radiation in the earth's atmosphere. *J. Atmos. Sci.*, **31**, 118–133.

Liou, K. N., 1973: A numerical experiment on Chandrasekhar's discrete-ordinate method for radiative transfer: Applications to cloudy and hazy atmospheres. *J. Atmos. Sci.*, **30**, 1303–1326.

——, 1974a: On the radiative properties of cirrus in the window region and their influence on remote sensing of the atmosphere. *J. Atmos. Sci.*, **31**, 522–532.

——, 1974b: Analytic two-stream and four-stream solutions for radiative transfer. *J. Atmos. Sci.*, **31**, 1473–1475.

Mueller, P. K., R. W. Mosley and L. B. Pierce, 1972: Chemical composition of Pasadena aerosol by particle size and time of day. IV. Carbonate and noncarbonate carbon content. *Aerosols and Atmospheric Chemistry*, G. M. Hidy, Ed., Academic Press, 295–300.

Novakov, T., P. K. Mueller, A. E. Alcocer and J. W. Otvos, 1972: Chemical composition of Pasadena aerosol by particle size and time of day. III. Chemical states of nitrogen and sulfur by photoelectron spectroscopy. *Aerosols and Atmospheric Chemistry*, G. M. Hidy, Ed., Academic Press, 285–294.

Pollack, J. B., O. B. Toon and B. N. Khare, 1973: Optical properties of some terrestrial rocks and glasses. *Icarus*, **19**, 372–389.

Rodgers, C. D., and C. D. Walshaw, 1966: The computation of infra-red cooling rate in planetary atmospheres. *Quart. J. Roy. Meteor. Soc.*, **92**, 67–92.

Schuetzle, D., 1972: Computer controlled high resolution mass spectrometric analysis of air pollutants. Ph.D. thesis, University of Washington, 96 pp.

Try, P. D., 1972: An investigation of the influence of aerosols on the solar radiation field and the heating of a multiple scattering polluted urban atmosphere. Ph.D. thesis, University of Washington, 180 pp.

Volz, F. E., 1972a: Infrared absorption by atmospheric aerosol substances. *J. Geophys. Res.*, **77**, 1017–1031.

——, 1972b: Infrared refractive index of atmospheric aerosol substances. *Appl. Opt.*, **11**, 755–759.

——, 1973: Infrared optical constants of ammonium sulfate, Sahara dust, volcanic pumice, and fly ash. *Appl. Opt.*, **12**, 564–568.

Wang, W. C., and G. A. Domoto, 1974: The radiative effect of aerosols in the earth's atmosphere. *J. Appl. Meteor.*, **13**, 521–534.

Whitby, K. T., R. B. Husar and B. Y. H. Liu, 1972: The aerosol size distribution of Los Angeles smog. *Aerosols and Atmospheric Chemistry*, G. M. Hidy, Ed., Academic Press, 237–264.

Yamamoto, G., M. Tanaka and S. Asano, 1970: Radiative transfer in the infrared region. *J. Atmos. Sci.*, **27**, 282–292.